A Radio Frequency He– Source and a Source of Negative Ions by Cesium Sputtering

J.H. Billen

November 1980

UWFDM-368

FUSION TECHNOLOGY INSTITUTE

UNIVERSITY OF WISCONSIN

MADISON WISCONSIN

A Radio Frequency He– Source and a Source of Negative Ions by Cesium Sputtering

J.H. Billen

Fusion Technology Institute
University of Wisconsin
1500 Engineering Drive
Madison, WI 53706

http://fti.neep.wisc.edu

November 1980

UWFDM-368

A RADIO FREQUENCY He^- SOURCE AND A SOURCE OF NEGATIVE IONS BY CESIUM SPUTTERING

James H. Billen
Dept. of Physics and Dept. of Nuclear Engineering
University of Wisconsin, Madison, WI 53706

Summary

Two sources of negative ions are described. An rf source produces up to 14 μA beams of He^- by charge exchange in Rb vapor. The other Source of Negative Ions by Cesium Sputtering (SNICS) produces a wide variety of negative ion beams in the μA range. Two important features of SNICS are its simple, compact construction and its very good beam emittance (2-4π mm mrad MeV$^{\frac{1}{2}}$). Both sources have lifetimes >200 hours and they are used extensively on the Wisconsin EN tandem.

Introduction

The production of negative ion beams for injection into tandem electrostatic accelerators has long been an important part of the research program at Wisconsin. Figure 1 shows schematically the ion source test stand for unpolarized beam development. The analyzing magnet (mass-energy product ~8 amu MeV) deflects through ±30° ion beams with energies of 20-30 keV. Mass resolution of the system is 1.5%. One of the beam lines is equipped with a device[1] to continuously scan and measure beam emittance.

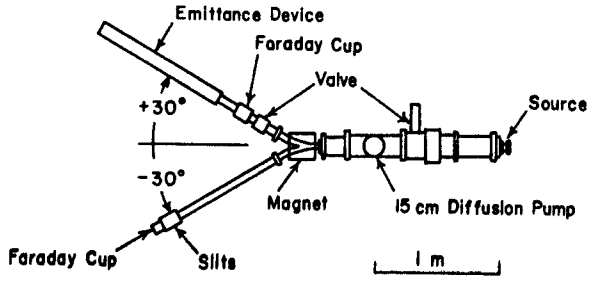

Fig. 1. Schematic of the ion source test stand.

He^- Source

In 1966 Rose, Tollefsrud, and Richards[2] developed the first source of He^- beams in the μA range. Figure 2 shows the essential features of an early version of the source. An rf discharge produces He^+ ions in a quartz bottle containing He gas at ~50 milliTorr. A

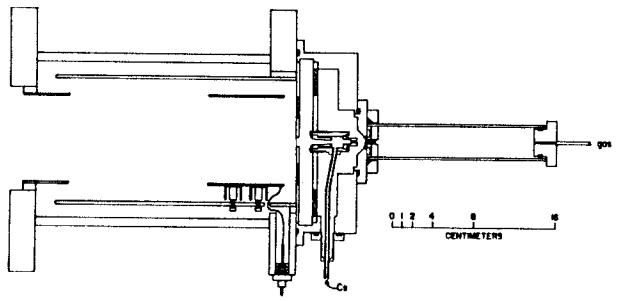

Fig. 2. An early version of the He^- source.

solenoid around the bottle produces an axial magnetic field of ~300 gauss on axis. The field confines electrons to spiral paths enhancing the plasma density. A ~5 kV potential difference across the discharge bottle establishes near the cathode extraction canal an electrical double layer which accelerates the He^+ ions through the canal and into a charge exchange cell containing cesium vapor. The mechanism for producing He^- by charge exchange in an alkali vapor is well-known and involves the two-step process first suggested by Donnally[3]:

$$He^+ + X^o \rightarrow He\ (1s\ 2s)\,^3S_1 + X^+$$

$$He\ (1s\ 2s)\,^3S_1 + X^o \rightarrow He^-\ (1s\ 2s\ 2p)\,^4P_{5/2} + X^+.$$

For Cs vapor at the appropriate target thickness and for ~6-keV He^+ ions about 1.4% of the incident He^+ ions convert to He^-.

The design attempted to reduce the flow of Cs vapor and retard its buildup on electrical insulators. A baffle separated the einzel lens from the charge exchange cell. The cell itself had a narrow acceptance solid angle and was the chief limitation on beam current. In addition, Cs vapor streaming from the charge exchange canal could enter the rf bottle and ultimately cause breakdown at the extraction canal.

Since that early design many new ideas and techniques to improve performance were tested and has resulted in an almost continual evolution of the He^- source. The first change was the removal of the einzel lens after the charge exchange region since the ~20 kV gap lens alone was sufficient for good He^- transmission through the tandem. The second change involved replacing the very small charge exchange cell with a Cs vapor stream at right angles to the He^+ beam.[4]

Today's version of the source is shown in Fig. 3. A diffusion pump-like stack that provided the Cs vapor jet was eventually removed in favor of the open-geometry recirculating alkali cell. In this arrangement Cs streams at right angles to the helium ion beam, condenses on the walls of the cell, and then flows back to the reservoir. A beam-heated washer between the charge exchange cell and extractor prevents the condensed alkali metal from migrating along surfaces to the extractor. Diffusion against the He gas flow is the only remaining mechanism by which alkali vapor can enter the discharge bottle.

In 1976 we began operating with Rb rather than Cs in the charge exchange cell. Measurements by Girnius and Anderson[5] indicated that the fraction of He^- ions to He^+ ions F_- for He^+ incident on rubidium is larger than the fraction F_- for He^+ incident on cesium[6] for all energies of the He^+ beam. Table I lists the maximum fraction F_- and the He^+ energy at which it occurs for all of the alkalis.

The lighter alkali vapors Na and K also have large He^- yields[7,8] but require higher operating temperature to give adequate vapor pressure and higher He^+ energies especially for sodium. Higher He^+ energy could be an advantage because in principle a larger space charge limited He^+ current is possible. But our experience is that operation with $\gtrsim$ 6 kV across the discharge bottle leads to electrical breakdown near the extractor, large return electron currents to the anode, and enhanced sputtering of the extraction electrode. To take advantage of the higher He^+ current possible at 12 kV with a Na charge exchange one might need a different type ion source (e.g. a duoplasmatron) from which one can extract the beam at higher energy. We find either Cs or Rb easier to handle than the other alkali metals because they melt at relatively low temperatures and can be poured into the loading

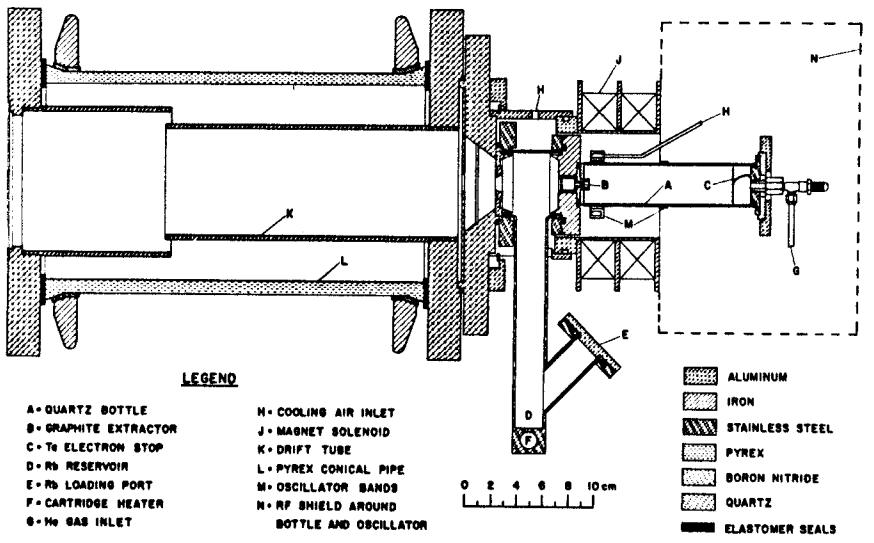

Fig. 3. Detail of the He^- source assembly. The quartz bottle assembly is held to the iron baseplate by spring loaded bolts not shown in the drawing. The Ta electron stop at the anode keeps the 40 W return electron beam from overheating the viton o-ring.

Table I

Maximum Conversion Fraction F_- for He^+ Incident on Alkali Vapors

Alkali	Max.F_- (%)	He^+ Energy (keV)	Reference
Li	0.6	12	D'yachkov & Zinenko(1971)
Na	1.7	12	D'yachkov & Zinenko(1971)
K	1.7	7.5	Ennis et al.(1967)
Rb	1.7	7	Girnius & Anderson(1976)
Cs	1.4	6	Schlachter et al. (1968)

port after filling the source with dry argon. Adequate vapor pressure of Rb occurs with temperatures of ~260°C at the reservoir and ~135°C on the walls of the exchange region. Air cooling suffices to remove the modest amount of power supplied to the reservoir. Viton o-rings are used for vacuum seals.

Figure 4 shows a comparison of the present quartz bottle and extractor geometry to that in use until 1975. In the early design on the left, a pair of quartz discs cemented to the inside of the quartz tube shielded the outer surface of the extractor. This shielding forces the plasma double layer to form in front of the opening in the extractor. However, because the available quartz tubes are not round, one could not ensure alignment of the hole in the quartz discs with the extraction electrode (which was clamped independently to the base plate). We also experienced problems with sparking through the zirconium-base cement. The cement was tedious to apply and required a thorough bake out before a new bottle could be used on the source. The design shown on the right in Fig. 4 eliminated these problems. We now fuse vacuum tight a quartz disc to the end of the quartz tube. A sleave of boron nitride fits between the extractor and the quartz disc and is positively aligned even if the quartz tube is out of round. The BN insulator also serves as the inner ring for a viton o-ring.

Sputtering of the iron extraction canals in use until recently limited lifetime to ~100 hours. Sputtered material coats the quartz tube reducing the rf power available to ionize He and also alters the potential in the region of the extractor. The notch between the two quartz discs and the complicated extractor shape shown on the left of Fig. 4 were attempts to retard the onset of electrical breakdown caused by the build-up of conducting material inside the quartz disc. These modifications helped only slightly, however, and we now use the simpler construction shown on the right of Fig. 4.

Previous experience with the source had indicated that the use of a ferromagnetic extraction electrode increased the yield of He^+ from the source, presumably by increasing the magnetic flux and hence the plasma density in the immediate vicinity of the extractor tip. We had been reluctant, therefore, to use a nonferrous extractor. Recently, with the geometry on the right in Fig. 4 (which has an iron base plate), we tested other cathode materials in search of one that sputters less readily than iron. With extractors of either molybdenum or graphite we obtained the same He^+ and He^- currents and emittance as we had with iron extractors. The Mo extractor sputtered rapidly and blackened the quartz tube in only a few hours. But a graphite cathode eroded much less than either Fe or Mo. Several days passed before the tube was coated appreciably. The rate of percentage mass loss for a graphite extractor was 8 times less than the rate for an iron extractor of the same size and shape (1.6 mm diameter, 12.7 mm long).

Our emittance measuring device quickly determines both the phase space area and the portion of the total beam included within a given brightness contour. Figure 5 shows phase space plots of a He^- beam for

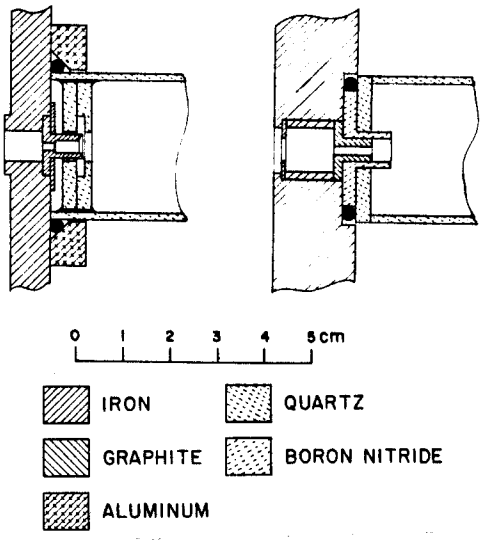

Fig. 4. Extraction geometry for an earlier source on the left and the present design on the right.

three different brightness contours. The shape of an emittance versus percent-of-beam curve resembles one of the solid curves of Fig. 6. For several He^+ beams with total currents between 80 μA and 330 μA, the emittance curves lie between the upper and lower solid curves. The He^- beam emittance lies between the upper and middle curves. Scattering in the charge exchange region is relatively unimportant, producing only a slight increase in the average emittance of He^- beams compared to He^+ beams. We have tested the source with three different alkali vapors K, Rb, and Cs and find no dependence of the He^- emittance on which alkali vapor is used for charge exchange.

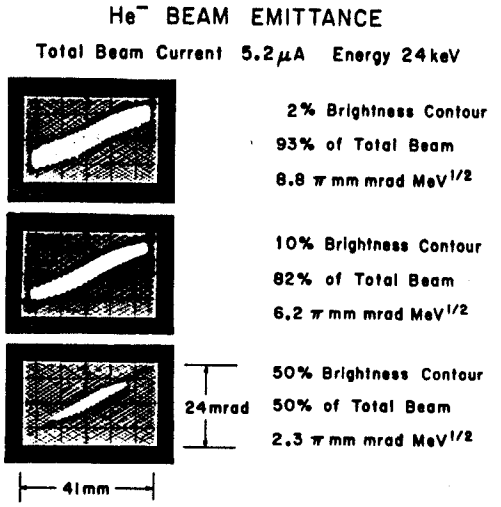

Fig. 5. He^- beam emittance for three different thresholds of brightness.

The range of measurements displayed in Fig. 6 corresponds to different sets of operating parameters and a wide range of beam currents. We have not yet searched systematically for a correlation between any single source parameter and emittance. The detailed shape of the plasma double layer near the extractor certainly influences the emittance. This shape depends upon many factors which include the anode-to-cathode voltage, geometry, pressure, magnetic field strength, and ion density. The distribution of sputtered material in the extraction region may also be important.

Table II lists typical operating and performance parameters for the He^- source. We now routinely obtain ~6 μA of He^- current, the record being 14.5 μA. Iron-constantan thermocouples measure the reservoir and exchange canal temperatures and a potentiometric controller maintains the 260°C temperature of the Rb reservoir independent of line voltage fluctuations.

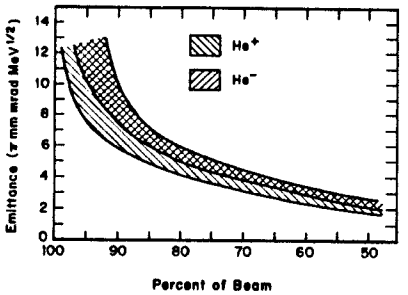

Fig. 6. Beam emittance vs. percent of total current.

Table II

Typical He^- Source Parameters

Oscillator Voltage	800 V
Current	260 mA
Extractor Voltage	5 kV
Current	8 mA
Axial Magnetic Field	300 G
Gap Voltage	20 kV
Rb Charge	10 g
Rb Reservoir Temperature	260°C
Exchange Canal Temperature	135°C
Pressure	~50 mTorr
Total Power Consumption	400 W
Operating Life	>200 h
He^- Current	6 μA
He^- Emittance (85%)	6.5 π mm mrad $MeV^{\frac{1}{2}}$
He^- Beam Energy	25 keV

Cooling air flow must be carefully controlled to maintain ~135°C on the walls of the charge exchange area. Too much cooling freezes Rb in the exchange canal and halts its recirculation. The pressure of ~50 mTorr is an estimate based upon flow considerations. The best indication of proper He pressure (and also purity) is the blue-green color of the discharge. A liquid-nitrogen cold trap removes most contaminants from the helium supply. Good performance results for very pure He gas at as low a pressure as possible without extinguishing the discharge.

SNICS

The source of negative ions by cesium sputtering (SNICS) has now been in routine use on the tandem since June, 1978. After a description of the design and operating principles of the source I will discuss performance characteristics and summarize our experience with different negative ion species. I will also present calculations of Cs^+ ion trajectories that seem to explain the erosion pattern of the sputter cathode. Early work on the source has been described in the literature.[9,10,11]

Figure 7 shows schematically the source and its acceleration and focussing components. Cesium vapor enters the source through a heated bellows type metering valve connected between a Cs oven and the bottom Cajon VCR gland. The five-turn helix of 1 mm W wire is hot enough to surface ionize Cs. The resulting Cs^+ beam of 3-5 mA bombards the sputter cathode which is coaxial with the ionizer and the anode aperture. The ionizer, housing, and a set of Ta heat shields (not shown) are all at anode potential. Sputtered negative ions of the cathode material accelerate across the 2-kV cathode-to-anode potential difference. The negative ion beam emerging from the anode aperture gains another 5 keV of energy in the first acceleration gap, and then enters an einzel lens. The beam gains 15 keV of energy in the final acceleration gap.

Table III lists typical operating and performance parameters for a 10-μA beam of Cu^-. Operating life is limited by consumption of the sputter cathode and is not related to the consumption of Cs. A 2-g charge of Cs can last several hundred hours as the source efficiently recycles Cs vapor. After enough Cs vapor to produce 3-5 mA of sputter cathode current has entered the ionizer region we often close the metering valve for periods of 20-30 hours and observe little decline in negative ion current. Negative ion output is insensitive either to the initial shape of the sputter cathode or to the anode-to-cathode spacing. There is also no advantage in biasing the W ionizer with respect to anode potential. A simpler version of

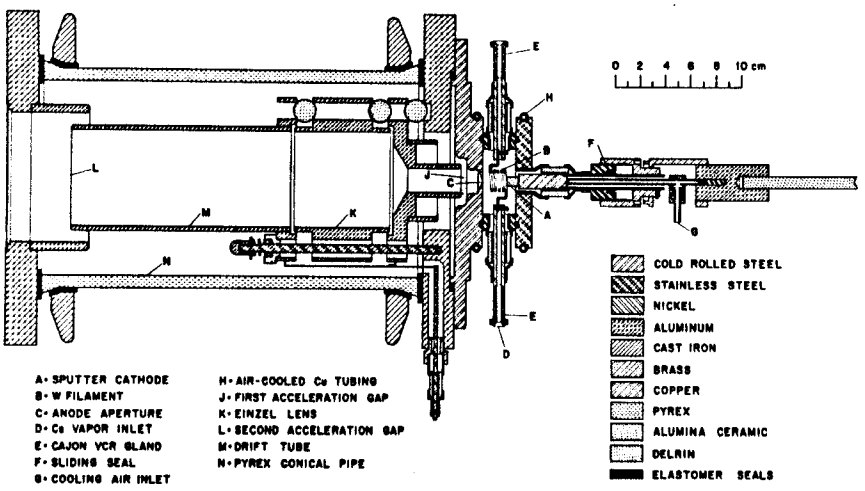

Fig. 7. Detail drawing of SNICS. The Ta heat shields around the ionizer filament and the Cs oven and metering valve are not shown.

Table III

SNICS Parameters for Cu^-

Ionizer Voltage	5 V
Current	30 A
Sputter Cathode Voltage	2 kV
Current	3 mA
Cs Charge	2 g
Cs Reservoir Temperature	250°C
Metering Valve Temperature	300°C
Anode to Cathode Distance	17 mm
Anode Aperture Diameter	1.5 mm
First Gap Voltage	5 kV
Second Gap Voltage	15 kV
Total Power Consumption	260 W
Operating Life	>250 h
Cu^- Current	10 μA
Cu^- Emittance (90%)	3.0 π mm mrad $MeV^{\frac{1}{2}}$
Cu^- Beam Energy	22 keV

SNICS would have a fixed-position cathode and only one leadthrough for the W filament. One might also eliminate the second gas inlet canal. Best performance is with Cs vapor alone. The presence of any of the gases we have tried (Ar, O_2, H_2) reduces dramatically the negative ion output. The very good beam emittance of 3π mm mrad $MeV^{\frac{1}{2}}$ is consistent with the pronounced axial erosion of the sputter cathode as illustrated in Fig. 8.

The initial attempt[10] to explain the axial erosion involved the focussing of plasma ions by the electric field and by the magnetic field produced by a dc current in the filament ionizer. We now know that axial erosion occurs even with ionizers that produce

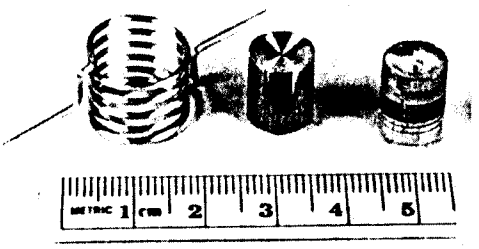

Fig. 8. Photograph of a W ionizer, an unused sputter cathode, and a cathode after several hours of running.

no magnetic field.[12] Other details of the erosion pattern of the sputter cathode suggested that the incident particles' trajectories originated directly from the hot W ionizer (rather than in a plasma). To check this possibility we calculated several hundred trajectories for Cs^+ ions produced on the hot tungsten surface. The electric potential used for these calculations resulted from a solution of Laplace's equation in cylindrical coordinates with Dirichlet boundary conditions as indicated in Fig. 9. We ignored the effects of space charge and of magnetic fields and for simplicity we considered five circular hoops in place of the helix.

Sample trajectories for Cs^+ ions originating on one of the hoops are shown in Fig. 9. The Cs^+ current density (and hence erosion) as a function of radial position on the face of the cathode is proportional to the number of trajectories whose end points lie within a particular annular zone divided by the area of the zone. For 250 trajectories with origins evenly distributed over all five hoops about 60% of the Cs^+ ions strike the flat face of the sputter cathode and the rest hit the side. Because of the difference in surface areas the face sputters ten times as rapidly as the side. Furthermore, the Cs^+ current density on the face is very strongly peaked on axis as shown in Fig. 10. Qualitative similarity between these predictions and actual erosion patterns is remarkable. The slight enhancement of the current density at about 2 mm arises from Cs^+ trajectories that begin on the three hoops farthest from the cathode. Such a shallow groove appears on our worn cathodes but with a spiral shape reflecting the actual geometry of the helix.

Table IV is a list of the negative ion beams obtained with SNICS. Most local demand has been for beams of Cu^- and Al_2^- for our radiation damage studies and $^{12}C^-$ and $^{13}C^-$ beams for nuclear spectroscopy. We have occasionally accelerated beams of $^7Li^-$, V^-, and Ni^-. We do not know the H_2 concentration in our stock of vanadium that is responsible for the intense H^- beam. A similar source[13] has produced negative ion beams of elements throughout the periodic table. Beam currents are generally higher than ours, but they are consistent with a factor of 2 difference in the exit aperture diameter. Emittance of the Pennsylvania

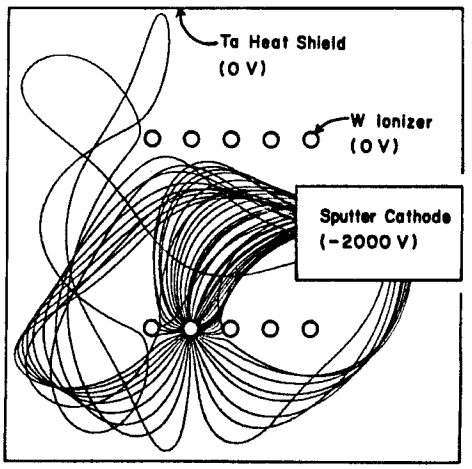

Fig. 9. Sample Cs^+ trajectories.

Table IV

Negative Ion Beams from SNICS

Cathode Material	Ion	Analyzed Current (μA)	Emittance 90% of beam (mm mrad MeV$^{\frac{1}{2}}$)
Vanadium	$^{1}H^{-}$	10	
Li_3N powder in Mo holder	$^{7}Li^{-}$	0.3	3.7π
LiH powder in Mo holder	$^{7}LiH_2^{-}$	0.15	
LiH powder + Pb binder	$^{7}Li^{-}$	0.1	
LaB_6 powder in Mo holder	$^{11}B^{-}$	0.02	
LaB_6 powder in Mo holder	$^{11}BO^{-}$	1.0	
Graphite	$^{12}C^{-}$	20	4.0π
Graphite	$^{12}C_2^{-}$	10	
^{13}C graphite powder in Mo	$^{13}C^{-}$	5	
(Various materials)	$^{16}O^{-}$	5	
Aluminum	$^{27}Al^{-}$	0.1	
Aluminum	$^{27}Al_2^{-}$	5.0	2.1π
Vanadium	$^{51}V^{-}$	4.0	
Nickel	$^{58}Ni^{-}$	6.0	
Copper	$^{63}Cu^{-}$	30	3.0π
Tantalum	Ta^{-}	0.25	
Tantalum	TaO^{-}	2.5	

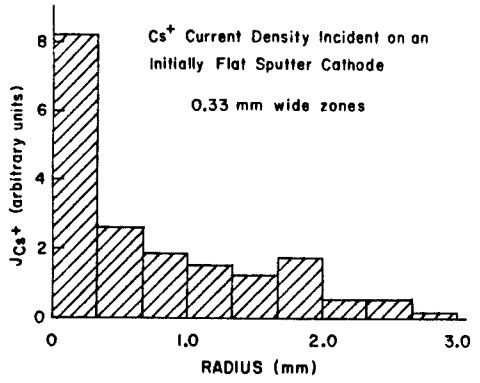

Fig. 10. Cs^+ current density on the face of the cathode.

source has not yet been measured. A cathode made from a mixture of B and Al powders yields a larger $^{11}B^{-}$ beam[13] than we have been able to produce.

Many solid cathodes yield O^{-} beams of several μA during the first few hours of operation as the Cs^+ beam sputters away an oxide layer. A sustained beam of O^{-} might be produced with a cathode made from any fine-grained metal powder (for example Al or Fe) or perhaps from certain oxide semiconductors.

Results with various lithium compounds are interesting. We have not tried Li metal because of its low melting temperature. So far Li_3N powder tamped into a Mo holder has yielded the most Li^{-} current. We chose this compound because of the large number of Li atoms per molecule and because nitrogen does not form a negative ion. Figure 11 compares mass spectra obtained with LiH powder with and without a binder of 25% (atomic) Pb powder. With LiH alone about 61% of the Li appears in the form of the molecular ion LiH_2^{-}, 27% appears as Li^{-}, and 12% appears as LiH^{-}. With the addition of a Pb binder almost 98% of the Li appears as the atomic negative ion Li^{-}. Presumably Pb, more electronegative than Li by 0.5 eV, ties up most of the hydrogen. The Li + Pb cathode produced only nA-intensity beams of Pb^{-} and of various molecular negative ions that involve Pb, H, Li, and O. The negative ion currents in Table IV that were produced by sputtering powdered materials can probably be pushed higher by more careful preparation of the cathodes. If trapped

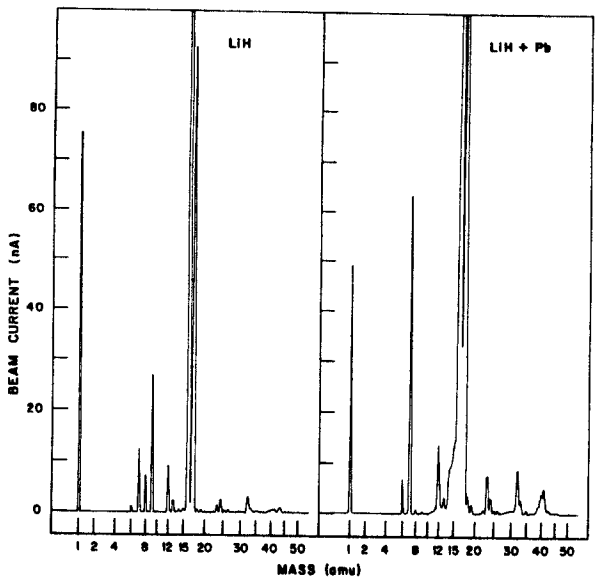

Fig. 11. Mass spectra of SNICS output for LiH and LiH + Pb cathodes.

air can be eliminated from the cathode then negative ion output will likely rise.

Acknowledgments

I wish to thank D. Wiltzius and National Electrostatics Corp. for the particle trajectory computer code. I also gratefully acknowledge Prof. H.T. Richards for many helpful discussions.

References

1. L.L. Ames, Nucl. Instrum. & Meth. 151 (1978) 363.
2. F.A. Rose, P.B. Tollefsrud and H.T. Richards, IEEE Trans. Nucl. Sci. NS-14 No. 3 (1967) 78.
3. B.L. Donnally and G. Thoeming, Phys. Rev. 159 (1967) 87.
4. H.T. Richards, Proceedings of the Symposium on Ion Sources and Formation of Ion Beams, BNL 50301 (Upton, N.Y. 1971) 295.
5. R.J. Girnius and L.W. Anderson, Nucl. Instrum. & Meth. 137 (1976) 373.
6. A.S. Schlachter, D.H. Loyd, P.J. Bjorkholm, L.W. Anderson and W. Haeberli, Phys. Rev. 174 (1968)201.
7. B.A. D'yachkov and V.I. Zinenko, Sov. Phys.-Tech. Phys. 16 (1971) 305.
8. R.M. Ennis, Jr., D.E. Schechter, G. Thoeming, D.B. Schlafke and B. Donnally, IEEE Trans. Nucl. Sci. NS-14 (1967) 75.
9. G.T. Caskey, R.A. Douglas, H.T. Richards and H.V. Smith, Jr., Bull. Am. Phys. Soc. 23 (1978) 541.
10. G.T. Caskey, R.A. Douglas, H.T. Richards and H.V. Smith, Jr., Nucl. Instrum. & Meth. 157 (1978) 1.
11. J.H. Billen and H.T. Richards, Proceedings of the Symposium of Northeastern Accelerator Personnel CONF-781051 (Oak Ridge, Tenn. 1978) 137.
12. R. Middleton, Proceedings of the Symposium of Northeastern Accelerator Personnel CONF-781051 (Oak Ridge, Tenn. 1978) 114.
13. R. Middleton, Proceedings of the Symposium of Northeastern Accelerator Personnel (Madison, Wis. 1980) to be published.